ISSN 1063-7826, Semiconductors, 2018, Vol. 52, No. 1, pp. 19–23. © Pleiades Publishing, Ltd., 2018.
Original Russian Text © V.N. Trukhin, A.D. Bouravleuv, I.A. Mustafin, G.E. Cirlin, J.P. Kakko, H. Lipsanen, 2018, published in Fizika i Tekhnika Poluprovodnikov, 2018, Vol. 52, No. 1, pp. 23–27.

XXI INTERNATIONAL SYMPOSIUM
"NANOPHYSICS AND NANOELECTRONICS",
NIZHNY NOVGOROD, MARCH 13–16, 2017

Ultrafast Dynamics of Photoinduced Electron–Hole Plasma in Semiconductor Nanowires

V. N. Trukhin[a]*, A. D. Bouravleuv[c], I. A. Mustafin[a, b], G. E. Cirlin[c], J. P. Kakko[d], and H. Lipsanen[d]

[a] *Ioffe Institute, St. Petersburg, 194021 Russia*
[b] *ITMO, St. Petersburg, 197101 Russia*
[c] *St. Petersburg Academic University, Russian Academy of Sciences, St. Petersburg, 194021 Russia*
[d] *Department of Electronics and Nanoengineering, Aalto University, FIN-02150 Espoo, Finland*
**e-mail: valera.truchin@mail.ioffe.ru*

Submitted April 27, 2017; accepted for publication May 12, 2017

Abstract—Experimental results obtained in a study of the effect of electron–hole plasma on the generation of terahertz (THz) radiation in semiconductor nanowires grown by metal-organic vapor-phase epitaxy (MOVPE) are presented. It is shown that the temporal dynamics of photoexcited charge carriers in semiconductor nanowires is determined by the transport of carriers, both electrons and holes, and by the time of capture of electrons and holes at surface levels.

DOI: 10.1134/S1063782618010244

1. INTRODUCTION

Semiconductor structures in the form of free-standing semiconductor nanowires (NWs) are among the most promising nano-objects for application in nanoelectronics, nanophotonics, and nanobioelectronics. The NWs are used to create ultrasensitive photodiodes [1], ultrahigh-density transistors [2], and emitters for the visible spectral range [3] and the THz range [4]. Therefore, the characterization of carrier dynamics in semiconductor NWs is of key importance for the application of these materials in the above fields of science and technology. The excitation of nonequilibrium electron–hole plasma in the local electric field of semiconductor NWs results in charge-carrier separation and, accordingly, changes the process in which terahertz radiation is generated. The temporal parameters of this change are determined by the charge-carrier relaxation and recombination processes and by charge-carrier transport.

2. SAMPLES AND EXPERIMENTAL

GaAs nanocrystals were grown on *n*-type GaAs (111)B substrates by metal-organic vapor-phase epitaxy (MOVPE). The chosen substrate orientation enables the growth of NWs perpendicularly to the surface. Growth was performed without the preliminary deposition of a catalyst layer, but with preliminary treatment of the substrates. For this purpose, a 40-nm-thick SiO_2 layer was initially deposited onto the substrate surface by plasma-enhanced chemical vapor deposition (PECVD). Further, ultrahigh-resolution electron-beam lithography was used to open windows in the oxide layer with a diameter of $d = 65$ or 100 nm with periods of 300, 600, 900, 1200, 1500, 1800, and 2100 nm. The opened apertures were situated at the vertices of an equilateral triangle. The NWs were grown directly in a horizontal atmospheric reactor. The height and diameter of the nanocrystals depended on the diameter of openings in the oxide layer and on the density of these. In particular, the actual diameter of the NWs was 120 nm for an opening diameter of 65 nm and 150 nm for $d = 100$ nm. The NW array with a given density was 400 × 400 μm in size.

The nanostructures were photoexcited with a titanium-sapphire laser generating optical pulses (wavelength 795 nm) with width of ~15 fs. The waveform of the terahertz pulse under the additional excitation of a NW with a femtosecond pulse was recorded by optical-pump terahertz-probe time-domain spectroscopy. This technique consists in examining the influence exerted by electron–hole plasma excited in a sample by a femtosecond optical pulse on the generation of a terahertz radiation. The experimental setup is shown schematically in Fig. 1. The main optical pulse of linearly polarized laser light is divided in two by the beam splitter BS1. The first optical pulse (pumping) is used to excite the sample under study and generate terahertz radiation in the sample. The second pulse (probe) serves to record the amplitude and phase of the terahertz radiation. The optical pump pulse passes

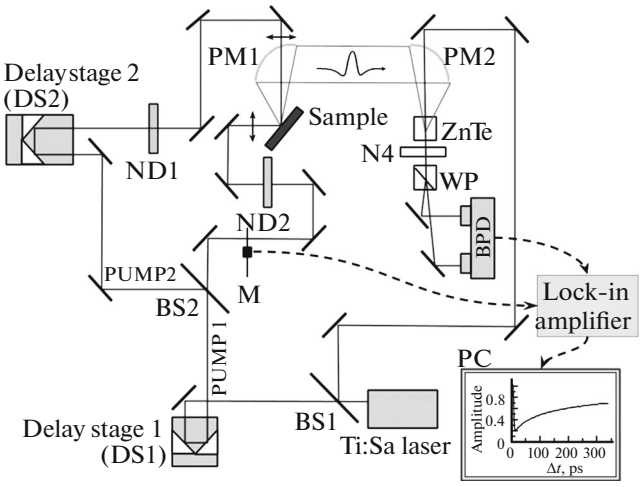

Fig. 1. Schematic of the experimental setup for time-domain spectroscopy. The THz pulse is recorded via electro-optical sampling with a ZnTe crystal (1 mm thick) used as the electro-optical crystal.

through the optical delay line DS1, which makes it possible to record the waveform of the terahertz pulse. Further, the optical pump pulse is divided in two by the beam splitter BS2. Accordingly, one of these pulses (PUMP1) is used to generate terahertz radiation, and the other (PUMP2) additionally excites the sample and creates electron–hole plasma. A time delay between the pulses PUMP1 and PUMP2 is created by the optical delay line DS2. Inclined incidence of light and the mirror configuration of recording THz radiation are used in the experiment. The optical pulse PUMP1 causing THz generation (to be recorded) is incident on the sample at an angle of 45° (the angle is chosen to be positive on the side of incidence of the PUMP1 pulse). The THz radiation is recorded at an angle of –45°. Naturally, for THz emission caused by the optical pulse PUMP2 not to be recorded by the receiving system, optical pulse PUMP2 is to be directed at the sample at an angle of –45°, so that its THz radiation does not propagate in the recording direction. This reduces the influence exerted by modulation with this THz pulse due to a change in the medium by the optical pulse PUMP1. The intensities of these light pulses are attenuated by neutral filters ND1 and ND2. The average powers of optical pulses PUMP1 and PUMP2 were 0.1 and 0.25–6 mW, respectively. To record the terahertz radiation generated under the excitation of a sample by a light pulse (PUMP1), it is modulated and the lock-in amplifier is synchronized by reference pulses at the modulation frequency. Modulation is performed by a chopper M. In the end, the terahertz radiation generated under the excitation of a sample by the light pulse PUMP2 should not be recorded by the receiving system if it is not modulated at the frequency of the chopper M. The THz radiation being generated is collected by parabolic mirrors PM1 and PM2 and focused onto a detector of coherent THz radiation, the role of which is played by an electro-optical ZnTe crystal. The setup employs the scheme of electro-optical time gating for the detection of coherent THz radiation. The interaction between the field of the THz wave and the probe light beam in the electro-optical crystal results in a change in the polarization state of the probe beam, which is detected by the optical system including a quarter-wave $\lambda/4$ plate, Wollastone prism WP, and a balanced photodiode detector BPD.

The output signal of the balanced detector is measured with a Signal Recovery 7265 lock-in amplifier at a modulation frequency of 1070 Hz. The 7265 lock-in amplifier is connected to a personal computer (PC) via the GPIB interface. The optical delay lines DS1 and DS2 are controlled by corresponding controllers, connected to the computer.

The signal from the balanced photodetector is further processed and the optical delay lines are controlled by a program designed to control the experiment developed on the basis of the LabView 7.1 platform.

3. RESULTS AND DISCUSSION

The generation of THz radiation in our samples may be associated with charge-carrier motion in the surface and contact fields, and also with ambipolar diffusion [4–6]. It should be emphasized that the contribution from ambipolar diffusion is insignificant if the wavelength of the excitation light exceeds the distance between the NWs. Figure 2 shows the time dependence of the maximum amplitude of the THz field for the nanostructure with d = 150 nm and a = 1200 nm. In these dependences, the THz field of the pulse being generated first falls after the electron–hole plasma is excited and then it is slowly restored. In the stage in which the efficiency of THz generation is restored, double-exponential restoration at a high excitation level is observed. Figure 3 shows similar dependences having a period of 600 nm between the nanocrystals. A similar situation is observed. Figure 4 shows the dependence of the maximum amplitude of the THz field at different excitation levels for a structure with nanocrystals 120 nm in diameter and a period of 1200 nm between these. It can be seen that the double-exponential restoration at a high excitation level is recorded at a substantially higher excitation intensity, compared with the structures having a nanocrystal diameter of 150 nm.

The magnified parts of the curves around the instant at which the pumping and probe pulses coincide are shown in Fig. 5 for the nanostructure with a = 1200 nm and in Fig. 6 for the nanostructure with a = 600 nm. The slight initial rise in the efficiency of THz generation is due to the influence exerted by modulation of the THz pulse generated by the pump pulse

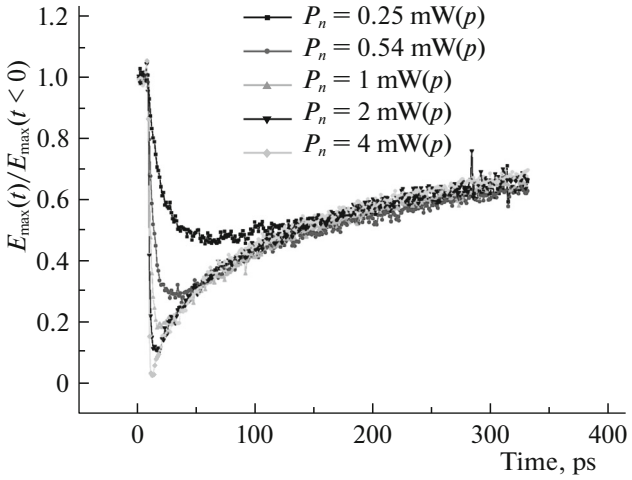

Fig. 2. Maximum amplitude of the THz field (normalized to the amplitude of the THz field at $t < 0$) vs. the delay between femtosecond pulses at various excitation levels P_n for the nanostructure with $d = 120$ nm and $a = 1200$ nm.

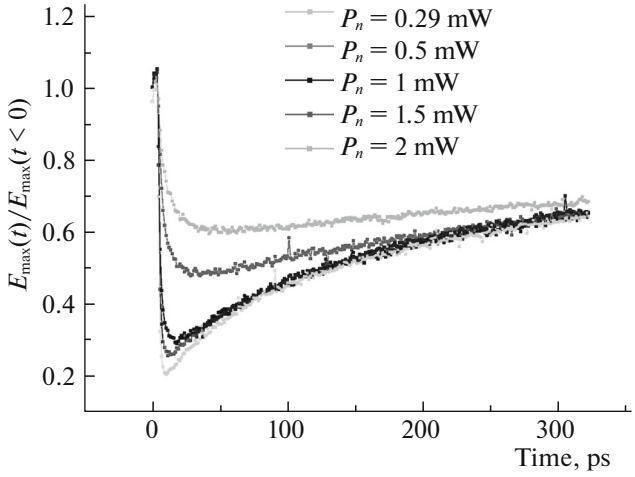

Fig. 3. Maximum amplitude of the THz field (normalized to the amplitude of the THz field at $t < 0$) vs. the delay between femtosecond pulses at various excitation levels P_n for the nanostructure with $d = 150$ nm and $a = 600$ nm.

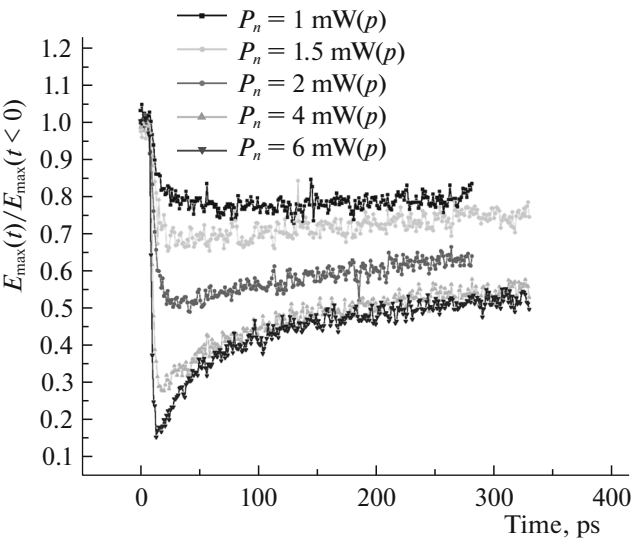

Fig. 4. Maximum amplitude of the THz field (normalized to the amplitude of the THz field at $t < 0$) vs. the delay between femtosecond pulses at various excitation levels P_n for the nanostructure with $d = 120$ nm and $a = 1200$ nm.

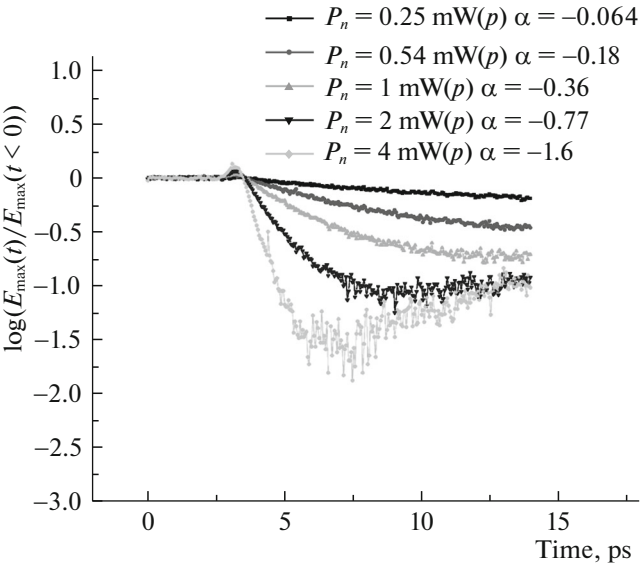

Fig. 5. Amplitude of the THz field vs. the delay between femtosecond pulses at various excitation levels P_n for the nanostructure with $d = 150$ nm and $a = 1200$ nm (α is the slope ratio at the beginning of the decay curve).

PUMP2. It can also be seen that the initial decay of the THz field occurs by the exponential law with a coefficient determined by the excitation level. For the structure with a period of 600 nm between the nanocrystals, the efficiency of THz generation decreases at a higher rate at the same excitation intensity.

The fall in the THz generation efficiency in GaAs-based semiconductor NWs is mostly due to shielding of the internal field in the nanocrystal (surface field near the upper face of the nanocrystal and the field of the n^+–n junction) due to the separation of nonequilibrium electrons and holes and to the transport of these in the surface and contact fields. The initial slope ratio can be used to estimate the time of charge-carrier momentum relaxation if we apply the concept that there is a capacitance of the depleted layer situated near the NW surface. (In what follows, we consider nanostructures with a NW period exceeding the wavelength of the excitation light on the assumption that the main contribution to THz generation is due to

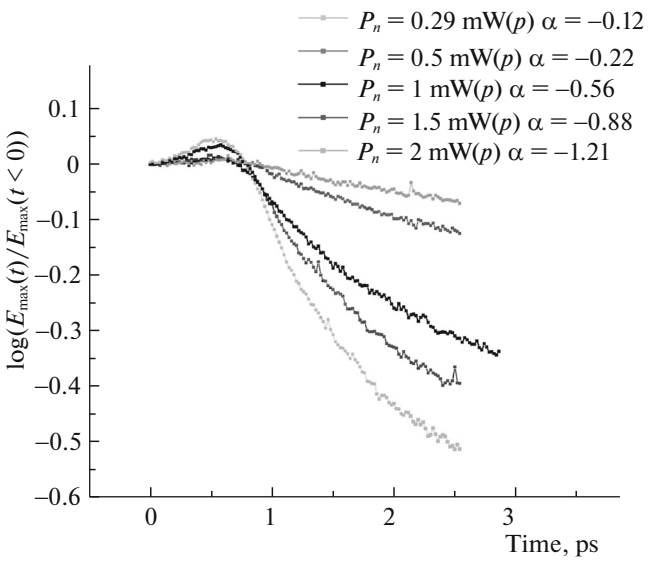

Fig. 6. Amplitude of the THz field vs. the delay between femtosecond pulses at various excitation levels P_n for the nanostructure with d = 150 nm and a = 600 nm (α is the slope ratio at the beginning of the decay curve).

carrier motion in the surface field near the upper NW face.) Charging of the depleted-layer capacitance by the current of nonequilibrium charge carriers can be represented as

$$\frac{dQ(t)}{dt} = \frac{dCV}{dt} = \frac{\varepsilon\varepsilon_0\eta S}{d}\frac{dV}{dt} = JS = eN(\mu_e + \mu_h)\left(\frac{V_0 - V}{d}\right)S. \quad (1)$$

Here, C is the capacitance of the depleted layer; J is the current density of nonequilibrium carriers; S is the NW cross section; V_0 is the surface electrostatic potential; V is the photovoltage; μ_e and μ_h are the electron and hole mobilities; N is the concentration of nonequilibrium carriers; ε is the dielectric constant of GaAs; and η is the correction to the capacitance with consideration for edge effects. Because the effective hole mass substantially exceeds the effective electron mass in gallium arsenide, the current of holes can be neglected. By solving Eq. (1), we can calculate the change in the local electric field to be

$$\frac{E_{max}(t)}{E_{max}(t<0)} = e^{-(e^2N\tau_s/m^*\varepsilon\varepsilon_0\eta)t}, \quad (2)$$

where τ_s is the time of electron momentum relaxation, and m^* is the effective electron mass.

The strength of the THz field generated in the course of the motion of nonequilibrium carriers in the surface or applied electric field is proportional to the electric-field strength [7]. Accordingly, the change in the generation efficiency of the THz field upon the excitation of electron–hole plasma will be correlated with a change in the local electric field. The estimated time of the electron-momentum relaxation is on the order of 65 fs, which is a reasonable value for gallium arsenide. As already noted, the efficiency of THz generation decreases faster at the same excitation intensity for a nanostructure with a period of 600 nm between the nanocrystals. Presumably, this is due to the contribution of the ambipolar-diffusion current, which appears in nanostructures with distances between NWs smaller than the wavelength of the excitation light, and the increase in the total photocurrent results in that the time derivative of the photovoltage grows [see formula (1)].

It can be seen in Figs. 2, 3, and 4 that, at a low excitation level, the efficiency of THz generation is restored in a single-exponential way with characteristic times of about 2000 ps. Without the excitation of electron–hole plasma in a NW, the nanocrystal is almost completely depleted of electrons, which all occupy surface levels. For a NW with a diameter of 150 nm, the band bending in the radial direction is 23 mV, i.e., it is on the order of kT, and the electric field at the lateral surface is ~10^3 V/cm (this estimate corresponds to the density of uncontrolled-impurity levels on the order of 10^{16} cm^{-3}). Therefore, electrons will move at a low excitation level along the nanocrystal in the surface electric field and be partly captured at surface levels at lateral NW faces, and, upon being captured, will continue to shield the internal field. In the radial direction, nonequilibrium electrons and holes will be separated in space. In the given case, the restoration time of the efficiency of THz generation will be determined by the capture of nonequilibrium holes at surface centers and by the nonradiative recombination of nonequilibrium carriers in the bulk.

It follows from the experimental results (Fig. 2) that, at an average power exceeding 1 mW (this approximately corresponds to a nonequilibrium charge-carrier concentration of 2 × 10^{15} cm^{-3}), double-exponential restoration of the efficiency of THz generation starts to be manifested, i.e., there appears a fast component. Possible fast-restoration mechanisms are in operation for the following reasons. First, the separation of nonequilibrium charge carriers in the radial direction at these excitation levels weakens the electric field in this direction, which removes the obstacle to the motion of photoexcited carriers toward the NW surface and to their capture at surface levels. This will lead to a fast partial decrease in the shielding of the longitudinal surface field by nonequilibrium electrons situated at the boundary of the depleted region and will restore the band bending in the radial direction in this region. The second reason is associated with the fact that the separation of nonequilibrium charge carriers in the direction of the [111] axis of a nanocrystal weakens the surface field in this direction to such an extent that the drift of holes toward the upper NW face falls and gives way to their diffusion in

the reverse direction. Their motion (in fact, this is partial recharging of the surface capacitance) should restore the internal field. The time of their displacement can be estimated by using the hole diffusion coefficient in bulk GaAs and the initial length of the depleted region at the upper NW face. The estimated hole diffusion time of ~20 ps corresponds to the time of the experimentally observed fast restoration kinetics. Further, there mostly occurs the capture of holes to surface levels occupied by electrons and the nonradiative recombination of nonequilibrium charge carriers in the NW bulk. Thus, the double-exponential restoration of the efficiency of THz generation is manifested when the concentration of photoexcited charge carriers is sufficient for substantial weakening of the local electric field in both the radial and longitudinal directions. Therefore, the high threshold for the appearance of fast restoration dynamics of THz generation for nanostructures with a nanocrystal diameter of 120 nm, compared with structures with a NW diameter of 150 nm (see Fig. 4), is presumably due to the Mie effect. This effect causes a resonant rise in the electromagnetic-field strength in the nanocrystal with $d = 150$ nm [5, 6], and, accordingly, a lower excitation level is required for fast dynamics to appear in this nanocrystal.

4. CONCLUSIONS

Thus, the influence exerted by electron–hole plasma on the generation of THz radiation in GaAs semiconductor nanowires was studied. It was shown that the temporal dynamics of photoexcited charge carriers in semiconductor nanowires is determined both by the fast motion of electrons in a local electric field (charging of the capacitance of the depleted surface layer) and their fast capture at surface centers and by the diffusion of holes (recharging of the capacitance) and the nonradiative recombination of nonequilibrium charge carriers in the bulk.

REFERENCES

1. L. Cao et al., Nat. Mater. **8**, 643 (2009).
2. K. Tomioka, M. Yoshimura, and T. Fukui, Nature **488**, 189 (2012).
3. X. F. Duan, Y. Huang, Y. Cui, J. F. Wang, and C. M. Lieber, Nature **409**, 66 (2001).
4. V. N. Trukhin, A. D. Bouravleuv, I. A. Mustafin, G. E. Cirlin, D. I. Kuritsyn, V. V. Rumyantsev, S. V. Morozov, J. P. Kakko, T. Huhtio, and H. Lipsanen, Semiconductors **50**, 1561 (2016).
5. V. N. Trukhin, A. D. Bouravleuv, I. A. Mustafin, J. P. Kakko, T. Huhtio, C. E. Cirlin, and H. Lipsanen, Appl. Phys. Lett. **106**, 252104 (2015).
6. V. N. Trukhin, A. D. Buravlev, A. I. Eliseev, I. A. Mustafin, A. V. Trukhin, J. P. Kakko, T. Huhtio, and H. Lipsanen, Opt. Spectrosc. **119**, 754 (2015).
7. V. N. Trukhin, A. V. Andrianov, and A. V. Zinov'ev, Phys. Rev. B **78**, 155325 (2008).

Translated by M. Tagirdzhanov